Journal of Marine Research, 45, 513–532, 1987

Journal of
MARINE RESEARCH

Volume 45, Number 3

What controls the rate of equatorial warm water mass formation?

by G. T. Csanady[1]

ABSTRACT

Equatorial warm water formation is one important factor in the mass balance of Tropical Surface Water (TSW) in the Atlantic Ocean; another is drainage by the North Brazilian Coastal Current (NBCC). Both are affected by the depth of the TSW layer at the western boundary: deepening of this layer increases the transport of the NBCC and reduces warm water mass formation by shortening the eastern upwelling zone. Strengthening westward wind-stress steepens the thermocline in the western sector of the equatorial band, enhances upwelling in the eastern sector, affecting mass balance on both counts. Recirculation of TSW via a loop containing the North Equatorial Counter Current (NECC), and inflow from the south at the eastern boundary are also important elements of this mass balance: they depend on the wind-stress field over a wider region.

The various elements of this mass balance are parameterized in terms of western boundary layer depth and wind-stress in the western sector. The resulting first order equation describes the response of the system to the annual cycle of wind-stress. With quantitative inputs typical of the equatorial Atlantic, output variables are simulated realistically: upwelling varies from 3 to 18 $\times$ 10^6 m^3/s, NBCC transport from 13 to 26 $\times$ 10^6 m^3/s, both in accord with observation, as is simulated storage, and TSW depth. An interesting finding is that the east-west length of the upwelling region varies relatively little while everything except storage varies in phase with the wind-stress (the storage lags by 2 months). The lesser variation of upwelling sector length comes about because the steepening of the thermocline in response to increasing wind-stress is accompanied by deepening in the western end, necessary to allow the escape of excess fluid.

The results show the interplay of wind-stress, upwelling and western boundary current transport in the control of the oceanic heat gain in the equatorial band.

1. Woods Hole Oceanographic Institution, Woods Hole, Massachusetts, 02543, U.S.A.

1. Introduction

The global thermodynamic cycle executed by the ocean, which results in the poleward transfer of heat, consists of poleward and equatorward transport legs, and of water mass conversion processes, both warm-to-cold at high latitudes, and cold-to-warm in the tropical and subtropical ocean. The waters of the ocean may be likened to the working fluid of a heat transfer device, e.g. a hot water home heating plant. As in such a device, the layers of the ocean actively participating in the process must go through a full cycle, lose heat to the atmosphere at high latitude, flow toward the equator, be restored to their original temperature in the tropical or subtropical ocean, and finally flow poleward again. Resistances to flow and heat transfer must be overcome, so that the process must be mechanically and thermally driven, by wind, convection, and solar heating. The resultant intensity of the cycle (the heat transported poleward) depends on an interplay between driving effects and resistances.

In general, we have a better appreciation of the driving effects, the wind stress, convection due to surface cooling, radiant heat input, than of the resistances. Unlike the case of a mechanical device, fluid friction is not the main resistance to poleward or equatorward transport: more powerful inertial effects are at work on a rotating globe, preventing the free movement of fluid masses across latitude circles. Another principal resistance is the stabilizing effect of surface heating: this must be counteracted by mechanical stirring in order to reach a significant quantity of fluid. A question of considerable importance is, how these resistances affect key elements of the global thermodynamic cycle.

An important contribution to oceanic heat transport comes from the formation of Tropical Surface Water (TSW) in the equatorial Atlantic, its northward transport by the western boundary current system and by surface wind drift, followed by the destruction of this water type under cold air outbreaks from the North American continent. The typical temperature of TSW is 27°C; upon its destruction it is presumably converted into eighteen degree water (Worthington, 1972). The rate of formation is of order 10^7 m^3 s^{-1}, (total equatorial upwelling rate, Broecker *et al.*, 1978; Wunsch, 1984), so that the half cycle just described is responsible for the poleward transfer of 90 degree-sverdrups or about 0.36 petawatt (10^{15} W). This compares with a global transfer of 3 to 4 petawatts (Carissimo *et al.*, 1985).

The two principal resistances to poleward heat transfer by the ocean, stability and inertial constraints, are likely to control the rate of equatorial warm water (TSW) formation and its poleward escape. Stability has to be overcome and cold fluid brought to the surface in a sufficiently large region, at a rapid enough rate to retain a large fraction of the heat received from the sun. Also, the TSW water mass forms near the equator and starts off with near-zero potential vorticity; it must be able to break the constraint imposed by the planetary vorticity gradient. In two previous articles (Csanady, 1984, 1985, to be referred to as C1 and C2 from here on) I have discussed these two processes individually. The conclusion of C1 was that, on account of the high

numerical value of nondimensional latent heat, large heat retention by the ocean occurs at low latitudes only where upwelling into the mixed layer takes place at a velocity of order 10^{-5} m s^{-1}: otherwise the radiant heat gained at the surface is transferred to the atmosphere. The discussion in C2 suggested, on the other hand, that escape transport northward, via the North Brazilian Coastal Current (NBCC), depends mainly on just how deep the equatorial TSW layer is at its western boundary, just prior to flowing into the NBCC.

Is there a connection between these two processes? There is good reason to suppose so. In a simple mass balance model developed below, the depth of the TSW layer at the western boundary also influences the rate of warm water mass formation by controlling the extent of the region where cold water reaches the surface. Increasing western layer depth leads to a reduced rate of TSW formation. With other conditions fixed, mass balance is then only possible for a specific value of layer depth at the western boundary, which brings about the escape rate equal to the total inflows, including the integrated upwelling rate, less any "storage" associated with changes in the depth of the TSW layer.

Two reviewers have disputed the notion that western boundary TSW layer depth can influence the length of the "eastern" sector where cold water is brought to the surface. One reviewer has pointed out that the eastern sector is of more or less constant length, and occupies the region of primarily meridional wind. He suggested that the coincidence may have an unknown dynamical reason. My thesis in the present paper is that the reason is the requirement to maintain mass balance. While the complexity of the wind field not explicitly considered in the simple model undoubtedly affects the details, the basic relationships remain. TSW forms where the mixed layer is shallow but it can escape only if it becomes deep enough near the western boundary to drive the western boundary current. A simple thought experiment is to imagine the NBCC suddenly shut off, while upwelling and warm water mass formation continue. Tropical surface water would pile up until it was deep enough everywhere to prevent entrainment of cold water from below; upwelling would then continue, but would merely recycle warm water. Radiant heat input would all be converted to latent heat of evaporated water. One could, of course, argue that some other gate would open for the escape of TSW, but then *its* physics would determine how much water the TSW layer would have to contain to keep mass balance, and how this would affect eastern sector oceanic heat retention.

A simple quantitative model of the mass balance feedback mechanism in question is constructed below. The escape rate of TSW is parameterized on the basis of results in C2. From dynamical balances an upwelling model is derived for the eastern equatorial Atlantic and the rate of TSW formation related to layer depth at the western boundary. This model also yields an estimate of the storage rate. Other inflows and outflows are prescribed on an empirical basis. The resulting model simulates the seasonal variation of TSW storage, thermocline tilt, and warm water mass formation

rate in a realistic manner and demonstrates that the formation and poleward transport of TSW depends on an interplay of the equatorial TSW layer and the western boundary current draining it. It also supplies a "dynamical" explanation for the near-constancy of eastern sector length.

The model glosses over several details, such as the prevalence of meridional winds in the eastern sector, and several of its submodels can be criticized. For example, the constant mixed layer depth assumption (for the eastern sector) may mask an important control on warm water mass formation due to stability. It would certainly be desirable to develop the model further and explore the effects of various complexities. The object of the present article is to make the case that the powerful constraint of continuity connects the various elements of the system considered, and to do this in as simple a way as possible.

2. Mass balance of TSW

The TSW layer is bounded from below by a sharp thermocline, wherein the temperature drops from 25 to 15 degrees in something like 50 meters. As Merle and Arnault (1985) point out, the result is an "almost perfect two-layer ocean" with the relatively large density anomaly of $\epsilon = \Delta\rho/\rho = 2.5 \times 10^{-3}$ across the interface. TSW covers the tropical Atlantic to about 30N and S. Here only its behavior in a narrow equatorial belt is of concern, say 5° each side of the equator, see Figure 1. This belt contains the entire equatorial upwelling zone, whether one defines it as the zone where surface divergence may be inferred from oceanic observations, or as the zone where satellite data show oceanic heat retention to be substantial. The depth of the TSW layer in this region ranges from 25 m in the east to 160 m in the west, with significant seasonal variations.

Circulation of TSW in a limited region such as the box in Figure 1 may be thought of as consisting of two components: a closed gyre or gyres, and throughflow connecting cross-boundary inflow to outflow, inflow including upwelling. This corresponds to the formal decomposition of the transport vector into nondivergent and nonvortical parts. The nonvortical transport satisfies mass balance, the nondivergent one the vorticity balance (Csanady, 1986). Here mass balance is of primary interest.

The Easterlies exert a stress of order $.5 \times 10^{-4}$ m^2 s^{-2} (in kinematic units, i.e., divided by water density) on the TSW layer. The result is often stated in terms of Ekman transport, which would give large outflow contributions across the zonal boundaries of the box in Figure 1. It must be remembered, however, that the scale-depth of the Ekman layer, $0.1\ u^*/f$ ($u^* = |\tau|^{1/2}$ = friction velocity, f = Coriolis parameter) is large near the equator, typically 70 m at 4°. Therefore the Ekman transport is distributed more or less evenly over the TSW layer, much as geostrophic transport. Where momentum advection and interface friction are negligible, the sum

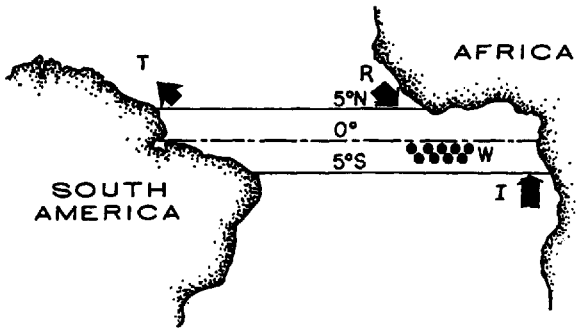

Figure 1. Near-equatorial band, within which mass balance of TSW is calculated. There is net inflow from the southern hemisphere, I, upwelling from the undercurrent, W, recirculation, R, and outflow via the NBCC, T.

of these two transports must satisfy the Sverdrup relationship:

$$\beta V = \text{curl}\, \tau \tag{1}$$

where $\beta = df/dy = 2.3 \times 10^{-11}$/m, s, τ is wind-stress vector, V meridional transport (velocity depth-integrated above the thermocline).

Wind-stress curl over the equatorial belt is weak and clockwise in the east, weak and anticlockwise in the west. Data on its magnitude are subject to large error bars (Hellerman and Rosenstein, 1983). With Eq. (1) they show equatorward Sverdrup transport of order 2 m^2/s, along most of the northern boundary of the belt in Figure 1. Integrated along this zonal boundary one finds equatorward transports from near zero to over 15×10^6 m^3/s, depending on season: little if any inflow in January, maximum in July. The Ekman transport is poleward, opposite to the Sverdrup transport, and about twice as large. Given the uncertainty of the curl estimates, one can only conclude that (if Eq. 1 applies) the geostrophic transport must be at least as large as the Ekman transport and be equatorward directed. In other words, the pressure gradient should more than balance the wind stress.

This conclusion is in excellent agreement with the surface dynamic height field calculated by Merle and Arnault (1985). Although a number of zonal troughs and ridges distort the lines of constant pressure, the zonal pressure gradient remains of the same order of magnitude over a much wider latitudinal band than is discussed here, opposing the westward wind stress everywhere. The magnitude of the surface elevation gradient is of order 0.7×10^{-7}, which just balances the typical westward directed wind stress of 0.5×10^{-4} m^2/s^2 where the TSW layer is 70 m deep. Seasonally, the pressure field varies with the wind field.

Sverdrup transport across the southern boundary of the box in Figure 1 is much weaker than across the northern boundary. Here a balance of wind stress and pressure gradient should hold, and transport should be entirely zonal. Drogue tracks and

ship-drift data show this clearly (Molinari, 1983; Richardson and McKee, 1984; Richardson and Wooding, 1985). TSW flows westward on a broad front toward the South American continent, where it is entrained into the surface portion of the NBCC (Metcalf and Stalcup, 1967; Richardson and McKee, 1984).

Both Eastern and Western Boundary Currents are important. At the western boundary the NBCC transports a large quantity of TSW northward, from about 10×10^6 m^3/s in the winter to perhaps three times as much in the summer (for references and discussion, see C2). The massive summer flow at least partially retroflects to form the North Equatorial Counter Current (NECC). The NECC constitutes the northern leg of the anticyclonic summer gyre driven by the wind stress curl, and it weakens eastward as streamlines bend southward to feed the interior Sverdrup transport. At the eastern boundary the southerly winds drive an equatorward extension of the Benguela Current and also cause coastal upwelling (Philander and Duing, 1979; Merle *et al.*, 1979). A broad and shallow drift of relatively cool water thus enters the TSW layer from the east, originating in the southern hemisphere. It is difficult to estimate the rate of this inflow, but, on account of its shallowness it can be no more than of order 3×10^6 m^3/s. Judging by surface temperatures and the surface dynamic height field, this inflow is also most pronounced in summer.

3. Box model of mass balance

Let the total quantity of TSW within the equatorial box be Q. The rate of change of this quantity equals the difference between inflow and outflow. According to the survey of the preceding section, inflows include: recirculation R via the anticyclonic gyre containing the NECC, entering through the eastern portion of the northern boundary; inflow I from the southern hemisphere, via the eastern boundary current, and area-integrated upwelling W through the thermocline. The only significant outflow is the transport T of the NBCC. The mass balance is therefore:

$$\frac{dQ}{dt} = R + I + W - T. \tag{2}$$

This equation becomes useful if one succeeds in relating its five terms to a smaller number of control variables. A simple scheme is to suppose the global wind-stress field over the equatorial box to be similar, any wind-related transports proportional to a seasonally varying characteristic wind stress. Recirculation and inflow then vary as:

$$R + I = (R_o + I_o)\frac{\tau_w}{\tau_o} \tag{3}$$

where R_o and I_o are the amplitudes of recirculation and southern inflow. τ_w is the westward zonal wind-stress in the western part of the equatorial belt, chosen as an index of seasonal variation, and τ_o is a constant scale value. The zonal wind stress will

be taken to vary sinusoidally with time:

$$\tau_w = \tau_a + \tau_s \cos \sigma t \tag{4}$$

where τ_a is the average stress, τ_s the fluctuation amplitude and the frequency σ is one cycle per year.

To represent the other terms in Eq. (2) simple submodels are required.

4. Escape transport submodel

Northward transport across 5N by the NBCC (T) will be parameterized using the inertial model of C2. The basic idealizations of this model were suggested by observations of Flagg *et al.* (1986) near 5N, just off the edge of the continental shelf. The surface layers of the NBCC appear here as an intrusion of low potential vorticity ($P = 0$) water, flanked on the land side by higher potential vorticity surface shelf waters, offshore by another, more extensive surface layer of high potential vorticity ($P \simeq 3 \cdot 10^{-7}$ m^{-1} s^{-1}). The latter "northern" water mass is in southwestward motion (counter to the NBCC) and in contact with a return flow leg of the intruding equatorial water mass. Model calculations showed this pattern of flow to be the consequence of inertial effects, potential vorticity and (approximate) energy conservation. The northern water mass blocks the intrusion, and causes outer streamlines of the NBCC to peel off one by one to form a southeastward flowing countercurrent, in confluence with some northern fluid. This combined return flow eventually becomes the North Equatorial Countercurrent (NECC) moving eastward between 4 and 8N.

The net conclusion is that equatorial water is allowed to escape northeastward across 5N at a rate T, which is limited by the key control variables of the system, mainly by the rest-depth ratio of the northern and equatorial water masses. For constant rest depth of the northern mass, the transport T varies with the depth h_o of the TSW layer at the equator, just outside the NBCC, approximately quadratically:

$$T = T_o \frac{h_o^2}{h_s^2} \tag{5}$$

where $T_o = 12.5 \cdot 10^6$ m^3 s^{-1}, $h_s = 100$ m.

5. Storage of TSW

Figure 2 from Fuglister's (1960) IGY Atlas illustrates the structure of the TSW layer at the equator in November. West of about 10W the thermocline tilts up to the east; farther east it is flat. Thermocline depth at the western boundary, outside the Western Boundary Current, is about 120 m, in the eastern constant depth region about 40 m. Sections taken at other times of the year show a similar structure, except that the thermocline tilt in the western section varies in response to the wind, becoming greatest

in July to September (Katz *et al.*, 1977; Philander and Duing, 1979; Merle, 1980a; Katz and Garzoli, 1982).

For the purpose of parameterizing TSW storage and upwelling rate the equatorial thermocline will be idealized as consisting of two sectors: a western one where the thermocline depth varies and an eastern one where it is constant. In the western sector there is no mass or momentum transfer across the thermocline; in the east upwelling and shear stress are important. The two regimes correspond almost exactly to the asymptotic states taken on by the equatorial mixed layer in Schopf and Cane's (1983) model study. In that study the mixed layer rapidly assumed one or the other asymptotic state, the deep one in the west, the shallow one in the east, with a short transition region.

The physical reason for the thermocline tilt in the western sector has been recognized early (Fofonoff and Montgomery, 1955; Veronis, 1960; Gill, 1975); it is the near-balance of pressure gradient and wind-stress. In a deep ocean, overlain by a shallow surface layer of depth h, buoyancy ϵg, such balance is expressed by:

$$\epsilon g h \frac{dh}{dx} = \tau_x \tag{6}$$

where τ_x is eastward wind stress. The assumptions underlying this relationship are that accelerations within the TSW layer and shear stress in the thermocline are negligible. As the results of Merle and Arnault (1985), quoted above, have shown, the same balance holds well away from the equator, where it also implies vanishing meridional transport. Putting $\epsilon g = 2.5 \cdot 10^{-2}$ m/s^2, $h = 100$ m, $\tau_x = -.6 \cdot 10^{-4}$ m^2 s^{-2} (mean wind stress in November) one finds $dh/dx = -2.4 \cdot 10^{-5}$. The thermocline tilt near 35W in Figure 2 (where $h = 100$ m) is of this magnitude, with a reasonable degree of smoothing.

The length of the western sector can be related to TSW layer depth at the western boundary. Upon integration, Eq. (6) yields:

$$h^2 = h_o^2 + \frac{2\tau_x}{\epsilon g} x \tag{7}$$

where h_o is again TSW layer depth at the western boundary, x the distance therefrom. For given westward wind stress $\tau_x = -\tau_w$ and buoyancy ϵg this formula shows that the western sector can only extend to a limiting distance x_l from the western boundary, where h vanishes:

$$x_l = \frac{\epsilon g h_o^2}{2\tau_w}. \tag{8}$$

Much the same x_l is found if one lets h become 25 or 40 m (the constant eastern sector value) instead of zero, at the junction of the two sectors.

With $\tau_w = 0.6 \cdot 10^{-4}$ m^2 s^{-2}, $h_o = 120$ m, $\epsilon g = 2.5 \cdot 10^{-2}$ m s^{-2} Eq. (8) yields $x_l =$

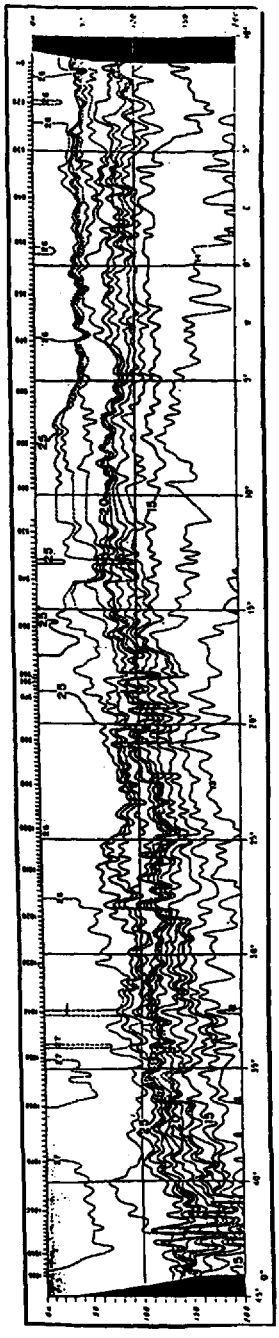

Figure 2. Typical temperature section along the equator in the Atlantic Ocean. The deep mixed layer of the western half contrasts sharply with the eastern half where the thermocline lies close to the surface. From Fuglister (1960).

3000 km, or about 27° longitude. In Figure 2 this would extend from the western boundary to 17W, in reasonable agreement with observation.

The length of the eastern sector, where upwelling takes place, is therefore $x_e = X - x_l$, where X is the coast to coast width of the basin, 52° longitude or 5700 km.

Deepening of the thermocline in response to increasing westward wind stress is tantamount to storage of TSW in the western sector. As Merle (1980b) has pointed out, this also implies seasonal heat storage when the Easterlies are strong, and the release of warm water when they weaken. The process will be quantified by taking the volume of the western sector between the western boundary and x_l as the only variable part of the storage. If the effective width of this sector is b, the volume stored is:

$$Q = b \int_o^{x_l} h \, dx. \tag{9}$$

Substituting from Eq. (7) the integral is readily evaluated:

$$Q = \frac{\epsilon g b h_o^3}{3\tau_w}. \tag{10}$$

As this result and Eq. (8) show, storage and the length of the western sector can both be related to wind stress τ_w and thermocline depth h_o at the western boundary.

6. Upwelling model

In the eastern sector Schopf and Cane's (1983) second asymptotic state will be supposed to prevail, with negligible zonal pressure gradient or horizontal advection of zonal momentum. The wind stress is then balanced by vertical momentum advection from the undercurrent, and shear stress at the bottom of the shallow, constant depth mixed layer. Off the equator, the Coriolis force of meridional transport has to be added, resulting in the depth-integrated momentum balance:

$$\beta y V + w_e \Delta u = -\tau_x + \tau_b \tag{11}$$

where w_e is entrainment (upwelling) velocity, Δu is velocity difference between the mixed layer and the undercurrent. Zonal transport is supposed nondivergent, so that the entrainment velocity is the divergence of meridional transport:

$$w_e = \frac{dV}{dy}. \tag{12}$$

The shear stress at the bottom of the mixed layer, τ_b, is taken to be a fixed fraction ϕ (say one half) of the surface stress:

$$-\tau_x + \tau_b = -\phi\tau_x. \tag{13}$$

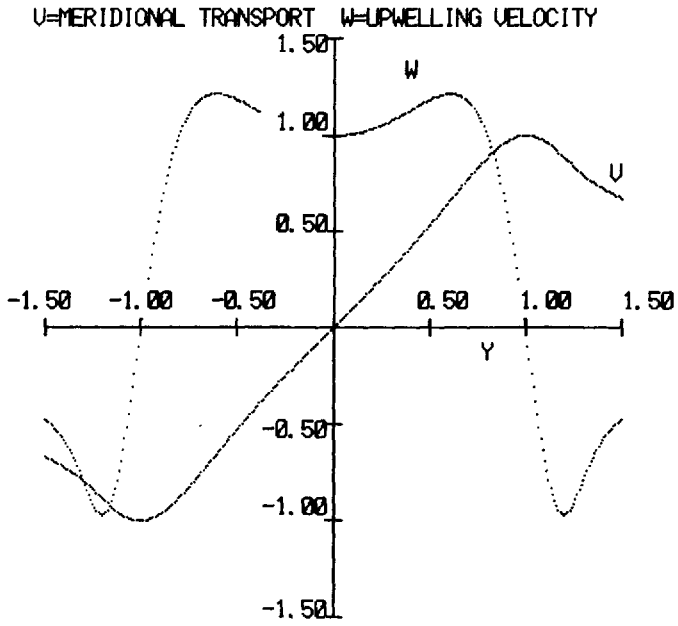

Figure 3. Nondimensional meridional transport, V, versus distance from the equator, for undercurrent model with $M = 0.72$ (nondimensional) or 150 km, and nondimensional upwelling velocity w_e. For scales see text or Table 1.

The typical undercurrent velocity distribution (for some examples see Gill, 1975) will be represented by

$$\Delta u = u_o \exp\left(-\frac{y^2}{M^2}\right) \tag{14}$$

where M is a meridional scale, typically 150 km, and $u_o = 1\ \mathrm{m\ s^{-1}}$.

Meridional transport at the equator is supposed to vanish:

$$V = 0 \qquad (y = 0). \tag{15}$$

Eq. (11) may now be integrated, with Eq. (15) as a boundary condition, and yields $V(y)$ and $w_e(y)$. Figure 3 shows the distribution of meridional transport and upwelling velocity, the units being

$$\begin{aligned} V &\quad -\phi\tau_x/\sqrt{u_o\beta} \\ w_e &\quad -\phi\tau_x/u_o \\ y &\quad \sqrt{u_o/\beta}. \end{aligned}$$

With $u_o = 1\ \mathrm{m\ s^{-1}}$, $\beta = 2.3 \cdot 10^{-11}\ \mathrm{m^{-1}\ s^{-1}}$, $-\phi\tau_x = 0.15 \cdot 10^{-4}\ \mathrm{m^2\ s^{-2}}$ these are $3\ \mathrm{m^2\ s^{-1}}$, $1.5 \cdot 10^{-5}\ \mathrm{m\ s^{-1}}$ and 209 km. Where w_e becomes negative, the theory does not

apply. The total upwelling rate integrated north to south is $1.53\,(-\phi\tau_x)/\sqrt{u_o\beta}$, or with typical values quoted above 6 $m^2\,s^{-1}$ per unit length of the eastern sector. Given the eastern sector length of $X - x_l$ one has the area-integrated upwelling rate

$$W = -\frac{2\phi\tau_x}{\sqrt{\beta u_o}}(X - x_l) \tag{16}$$

which amounts to $12 \cdot 10^6$ $m^3\,s^{-1}$ with the typical values quoted above and $X - x_l =$ 2000 km.

In this equation τ_x stands for wind stress in the eastern sector. Earlier, other quantities were parameterized in terms of the western sector wind stress, τ_w (positive westward) which is about a factor or two greater. The difference can be absorbed in the factor ϕ. Also substituting for x_l from Eq. (8) one has

$$W = \frac{2\phi\tau_w X}{\sqrt{\beta u_o}} - \frac{\phi\,\epsilon g h_o^2}{\sqrt{\beta u_o}}. \tag{17}$$

The factor ϕ becomes now about .25, allowing both for east-west differences in wind stress and momentum transfer through the thermocline. The result is an expression of the integrated upwelling rate W again in terms of τ_w and h_o.

7. Annual cycle of storage, upwelling and escape

With all terms of the mass balance, Eq. (2), now expressed in terms of h_o or τ_w, the response of the equatorial TSW layer to the annual cycle of wind stress may be examined. Upon substitution of the various parameterization schemes Eq. (2) becomes:

$$\frac{d}{dt}\left(\frac{\epsilon g b h_o^3}{3\tau_w}\right) = (R_o + I_o)\frac{\tau_w}{\tau_o} + \frac{2\phi\tau_w X}{\sqrt{\beta u_o}} - \frac{\phi\epsilon g h_o^2}{\sqrt{\beta u_o}} - T_o\frac{h_o^2}{h_s^2}. \tag{18}$$

In this equation the quantities ϵg, b, $R_o + I_o$, ϕ, u_o, T_o and suitably chosen scales of depth, h_s, wind stress, τ_o and time, t_s will be regarded constant. These are listed in Table 1. The choices of some have been discussed before. The time scale $t_s = u_o h_s/\tau_o$ yields convenient constants in the nondimensional form of Eq. (18). The annual cycle of wind stress, described by Eq. (4), contains two further constants, also listed in Table 1.

The following nondimensional dependent and independent variables suggest themselves:

$$E = \frac{h_o^2}{h_s^2} \qquad S = \frac{\tau_w}{\tau_o} \qquad t^* = \frac{t}{t_s} \qquad Q^* = \frac{E^{3/2}}{S}. \tag{19}$$

The different terms of Eq. (18) contain these variables multiplied by constants of the

Table 1. Parameters used in standard model calculation.

buoyancy, ϵg	$2.5 \cdot 10^{-2}$ m s^{-2}
meridional width, b	$1.1 \cdot 10^{6}$ m
recirculation and inflow amplitude, $R_o + I_o$	$8.75 \cdot 10^{6}$ m^3 s^{-1}
stress factor, ϕ	0.25
undercurrent velocity amplitude, u_o	1 m s^{-1}
escape transport amplitude, T_o	$12.5 \cdot 10^{6}$ m^3 s^{-1}
depth scale, h_s	100 m
wind-stress scale, τ_o	$0.5 \cdot 10^{-4}$ m^2 s^{-2}
time scale, $t_s = u_o h_s/\tau_o$	$2 \cdot 10^{6}$ s
transport scale, T_s	$91.67 \cdot 10^{6}$ m^3 s^{-1}
average wind stress, τ_a	$0.55 \cdot 10^{-4}$ m^2 s^{-2}
wind stress fluctuation amplitude, τ_s	$0.25 \cdot 10^{-4}$ m^2 s^{-2}
planetary vorticity gradient, β	$2.3 \cdot 10^{-11}$ m^{-2} s^{-1}
equatorial distance scale, x_s	$2.5 \cdot 10^{6}$ m
length of equatorial band, X	$5.7 \cdot 10^{6}$ m
storage scale, Q_s	$1.833 \cdot 10^{14}$ m^3

dimension L^3/T. The storage term on the left has the multiplier:

$$T_s = \frac{\epsilon g b h_s^3}{3 t_s \tau_o} = 91.67 \cdot 10^{6} \text{ m}^3 \text{ s}^{-1}$$

given the constants in Table 1. This is a scale of transports and also a measure of the storage capacity of the equatorial TSW layer over time scale t_s. It is proportional to b, the effective meridional extent of the storage zone. The value listed in Table 1 for b is the width of the 5N to S band, a possible overestimate in view of the fact that off-equatorial storage may change less. Dividing Eq. (18) through by T_s yields scaled values of $(R_o + I_o)$, T_o, etc. on the right.

With other parameters as listed, Eqs. (18) and (4) become with this scaling and dropping the stars from t^* and Q^*:

$$\frac{dQ}{dt} = \frac{d}{dt}\left(\frac{E^{3/2}}{S}\right) = 0.4196\, S - 0.2730\, E \tag{20}$$

$$S = 1.1 + 0.5 \cos(0.4t). \tag{21}$$

These two equations are readily integrated using a marching procedure from $t = 0$, with an arbitrary start $Q = 1$. As Figure 4 shows, a stable equilibrium cycle is reached within a year or so. The dimensional storage is Q times the storage scale $Q_s = T_s t_s = 1.833 \cdot 10^{14}$ m^3. The seasonal variation of Q seen in Figure 4 corresponds to about $0.73 \cdot 10^{14}$ m^3 difference peak to peak.

The escape transport is E times $T_o = 12.5 \cdot 10^{6}$ m^3 s^{-1}, varying according to Figure 4 between 13 and $26 \cdot 10^{6}$ m^3 s^{-1}. Figure 5 also shows the nondimensional western sector

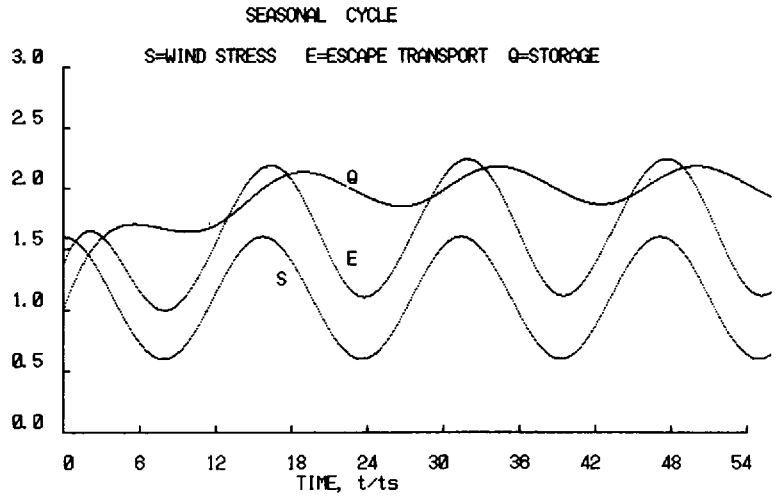

Figure 4. Seasonal oscillation of storage Q and escape transport E for sinusoidally varying wind stress, S, standard cycle. Parameters and scales are given in Table 1.

length (equal to E/S): the dimensional value x_l is the equatorial distance scale x_s = $2.5 \cdot 10^6$ m times the quantity taken from the figure. This varies between 3.25 and $4.5 \cdot 10^6$ m, or relatively less than other quantities. The nondimensional upwelling rate is $W = 0.324\ S - 0.142\ E$, which is a smaller quantity so that its fourfold multiple is shown. The dimensional upwelling rate is W times $T_s = 91.67 \cdot 10^6\ m^3\ s^{-1}$, varying from 3 to $18 \cdot 10^6\ m^3\ s^{-1}$.

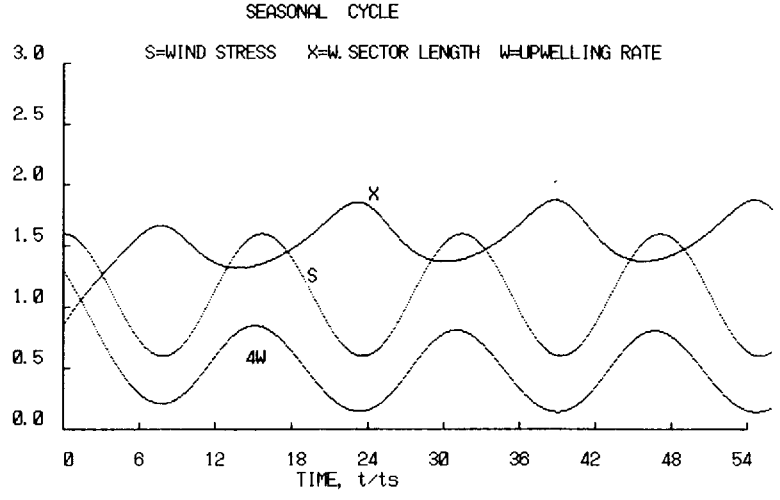

Figure 5. Seasonal variation of western sector length x_l and upwelling rate W in standard cycle.

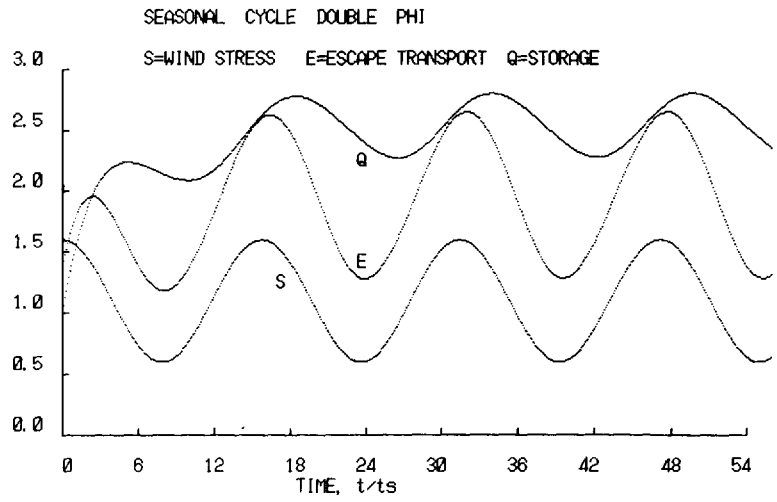

Figure 6. Modified seasonal cycle: constant ϕ doubled. This is equivalent to neglecting Reynolds stress in the eastern sector thermocline. Figure shows storage and escape transport, with wind stress repeated for reference.

The quantitative results are all in reasonably good agreement with the observed cycle of thermocline depth, upwelling rate, escape transport and storage (for the latter see Merle, 1980a,b). The variation in the length of the western sector is somewhat greater than observed, but it is still acceptably small. The lesser variability of x comes about because, when the increasing wind stress makes the western sector thermocline steeper, the western end has to become simultaneously deeper to allow larger escape transport. These two factors have opposite effects on x_I and partially cancel. The phase relationships are also more or less correct, W and E being nearly in phase with wind stress, while x_I is nearly in counterphase, and the storage lags about 2 months.

8. Tweaking the model

The annual cycle just calculated is relatively robust in the sense that changes in the less certain parameters do not qualitatively modify it. Reducing the amplitude of recirculation and inflow (which in the above calculations peaks at $14 \cdot 10^6$ m^3 s^{-1}) to zero makes little difference. Doubling the value of ϕ (i.e., supposing eastern sector wind stress the same as in the western sector, or alternatively supposing shear stress in the eastern sector thermocline zero) has more effect, Figures 6 and 7: escape transport increases by 15%, storage by 25%, western sector length also by 15%. Upwelling rate increases on the average, also by something like 15%, but its annual cycle shows a reduction in northern winter, substantial increase in summer.

Doubling the length of the basin to Pacific dimensions ($11.4 \cdot 10^6$ m) doubles

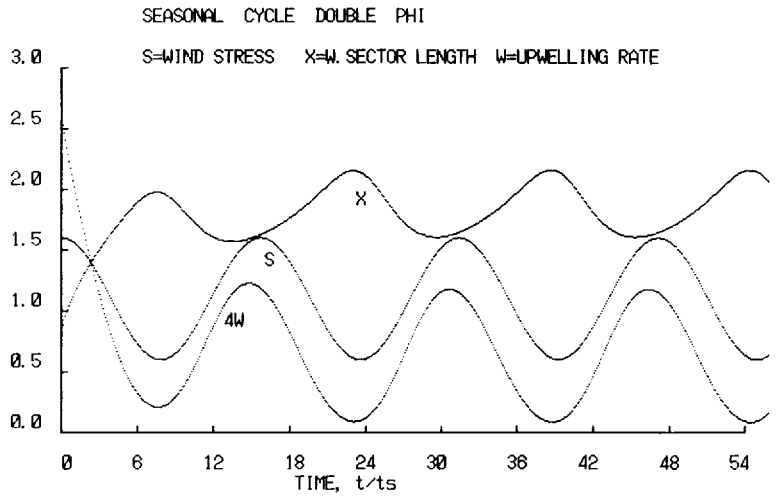

Figure 7. As previous figure, showing western sector length and upwelling rate.

everything in a first approximation, with escape rate and western sector length less than doubled, storage and upwelling more than doubled (Figs. 8 and 9).

Most interesting is the effect of a two-year modulation of the wind stress according to the formula:

$$S = 0.9 + 0.5 \cos(0.4t) + 0.2 \sin(0.2t) \tag{22}$$

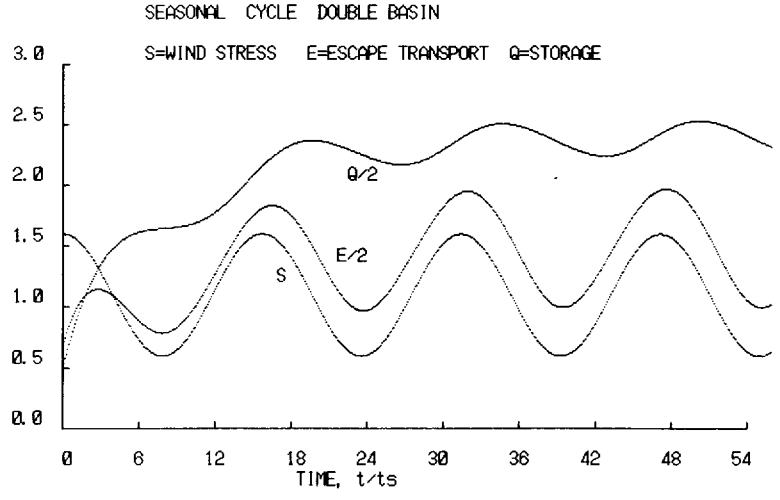

Figure 8. Standard cycle in an equatorial basin twice the zonal length of the Atlantic; storage and escape transport.

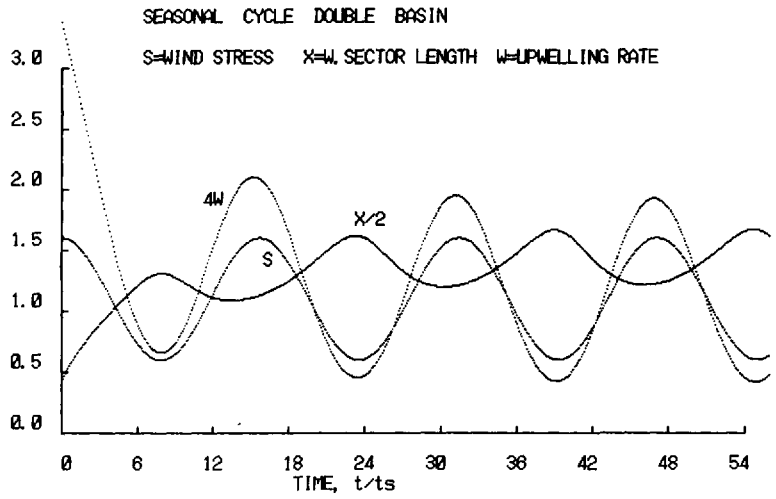

Figure 9. As previous figure, showing western sector length and upwelling rate.

which takes the place of Eq. 21. Every second year the wind stress is reduced, most severely in northern winter. Escape rate and storage change less than proportionately, and so does upwelling rate and western sector length, except that every second northern winter an "El Niño" occurs; the eastern sector disappears (x_I becomes equal to X) and warm water mass formation ceases ($W = 0$), see Figures 10 and 11.

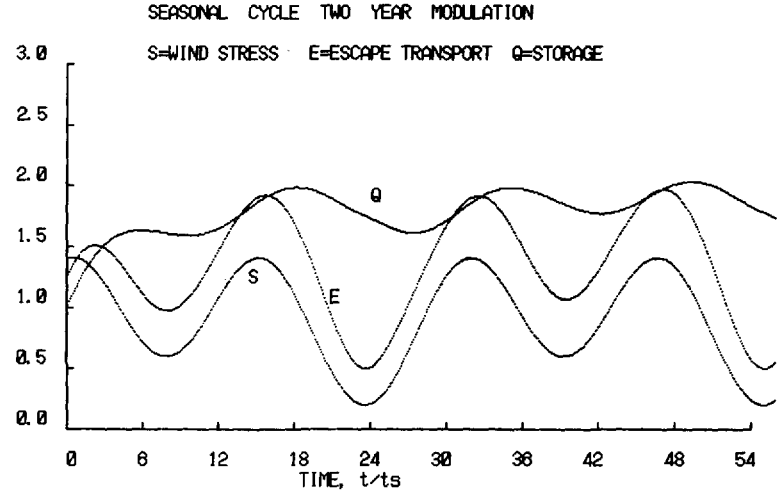

Figure 10. Wind stress cycle with two year modulation, the stress dropping in northern winter to a low value. Figure shows storage and escape transport, not dramatically different from standard cycle.

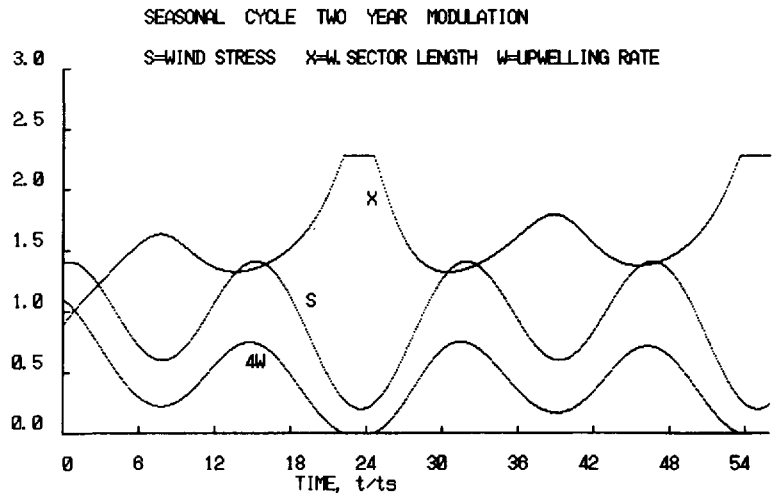

Figure 11. As previous figure, showing western sector length and upwelling rate. An "El Niño" occurs in northern winter, when the eastern sector thermocline deepens and warm water formation ceases.

9. Conclusion

The above model has a number of shortcomings, as already pointed out. Even as a box-model it is a damped version of reality, ignoring the equatorial Kelvin wave by which the system adjusts to changes in forcing. With all its shortcomings, however, the model realistically simulates the annual cycle of formation, storage and release of tropical surface water. It is, of course, a gross oversimplification to represent meteorological forcing over a wide region by a single variable, the characteristic wind stress, and the equatorial pressure field by another, thermocline depth at the western boundary. However, these very simplifications should make the point crystal clear that the escape rate (the breaking of the planetary vorticity constraint) has to be quantified, related to the parameters of the system, presumably to thermocline depth and topography. Without such a relationship the problem of mass balance in oceanic gyres is not well posed, as is evident from the behavior of models that lack it (e.g., Schopf and Cane, 1983) or from the measures modelers have to introduce at boundaries (e.g., Philander and Pacanowski, 1980).

Unfortunately, our understanding of western boundary current behavior is so rudimentary that no parameterization scheme has so far been suggested for "cross-gyre" transport. The crude stab made at this problem above should underline the need for a more solid conceptual basis of western boundary current dynamics.

Acknowledgments. The work described herein has been supported by the Office of Naval Research, Contract No. N00014-82-C-0019, NR 083-004. I am indebted to the referees for their very useful comments, and to Jacques Merle for some remarks on El Niño, which prompted

the model runs with two-year modulation. This is contribution number 6040 of the Woods Hole Oceanographic Institution.

REFERENCES

Broecker, W. S., P. H. Peng and M. Stuiver. 1978. An estimate of the upwelling rate in the equatorial Atlantic based on the distribution of bomb radiocarbon. J. Geophys. Res., *83,* 6179–6186.

Carissimo, B. C., A. H. Oort and T. H. Vonder Haar. 1985. Estimating the meridional energy transports in the atmosphere and ocean. J. Phys. Oceanogr., *15,* 82–91.

Csanady, G. T. 1984. Warm water mass formation. J. Phys. Oceanogr., *14,* 264–275.

—— 1985. A zero potential vorticity model of the North Brazilian Coastal Current. J. Mar. Res., *43,* 553–579.

—— 1986. On cross gyre transports. J. Phys. Oceanogr., *16,* 1703–1711.

Flagg, C. N., R. L. Gordon and S. McDowell. 1986. Hydrographic and current observations on the continental slope and shelf of the western equatorial Atlantic. J. Phys. Oceanogr., *16,* 1412–1429.

Fofonoff, N. P. and R. B. Montgomery. 1955. The equatorial current in the light of the vorticity equation. Tellus, *7,* 518–521.

Fuglister, F. C. 1960. Atlantic Ocean Atlas of Temperature and Salinity Profiles and Data from the International Geophysical Year of 1957–58, WHOI, Woods Hole, MA, 209 pp.

Gill, A. E. 1975. Models of equatorial currents, *in* Numerical Models of Ocean Circulation," pp. 181–203, Nat. Acad. Sci., Washington, DC, 364 pp.

Hellerman, S. and M. Rosenstein. 1983. Normal monthly wind stress over the world ocean with error estimates. J. Phys. Oceanogr., *13,* 1093–1106.

Katz, E. J., R. Belevich, J. Bruce, V. Bubnov, J. Cochrane, W. Duing, P. Hisard, H. U. Lass, J. Meincke, A. De Mequita, L. Miller and A. Rybnikov. 1977. Zonal pressure gradient along the equatorial Atlantic. J. Mar. Res., *35,* 293–307.

Katz, E. J. and S. L. Garzoli. 1982. Response of the western equatorial Atlantic Ocean to an annual wind cycle. J. Mar. Res., *40*(Supp.), 307–327.

Merle, J. 1980a. Seasonal heat budget in the equatorial Atlantic Ocean. J. Phys. Oceanogr., *10,* 464–469.

—— 1980b. Seasonal variability of heat storage in the tropical Atlantic Ocean. Oceanolog. Acta, *3,* 455–463.

Merle, J. and S. Arnault. 1985. Seasonal variability of the surface dynamic topography in the tropical Atlantic Ocean. J. Mar. Res., *43,* 267–288.

Merle, J., M. Fieux and P. Hisard. 1979. Annual signal and interannual anomalies of sea surface temperatures in the eastern equatorial Atlantic Ocean. Deep-Sea Res., Gate Suppl. II, *26,* 77–102.

Metcalf, W. G. and M. C. Stalcup. 1967. Origin of the Atlantic equatorial undercurrent. J. Geophys. Res., *72,* 4959–4975.

Molinari, R. L. 1983. Observations of near-surface currents and temperatures in the central and western tropical Atlantic Ocean. J. Geophys. Res., *88,* 4433–4438.

Philander, G. and W. Duing. 1979. The oceanic circulation of the tropical Atlantic and its variability as observed during GATE. Deep-Sea Res., GATE Suppl. *2,* 1–27.

Philander, S. G. H. and R. C. Pacanowski. 1980. The generation and decay of equatorial currents. J. Geophys. Res., *85,* 1123–1136.

Richardson, P. L. and T. K. McKee. 1984. Average seasonal variation of the Atlantic North Equatorial Countercurrent from ship drift data. J. Phys. Oceanogr., *14,* 1226–1238.

Richardson, P. L. and C. M. Wooding. 1985. Surface drifter measurements in the Atlantic North Equatorial Countercurrent 1983–1985. Technical Report WHOI-85-31, Woods Hole Oceanographic Institution, 117 pp.

Schopf, P. S. and M. A. Cane. 1983. On equatorial dynamics, mixed layer physics, and sea surface temperature. J. Phys. Oceanogr., *13,* 917–935.

Veronis, G. 1960. An approximate theoretical analysis of the equatorial undercurrent. Deep-Sea Res., *6,* 318–327.

Worthington, L. V. 1972. Negative oceanic heat flux as a cause of water mass formation. J. Phys. Oceanogr., *2,* 205–211.

Wunsch, C. 1984. An estimate of the upwelling rate in the equatorial Atlantic based on the distribution of bomb radiocarbon and quasigeostrophic dynamics. J. Geophys. Res., *89,* 7971–7978.

Received: *13 September, 1985;* revised: *21 April, 1987.*